The Structure and Biochemistry of NADH-Dependent Cytochrome b_5 Reductase Are Now Consistent†

Maria C. Bewley,*,‡ Christopher C. Marohnic,§ and Michael J. Barber§,||

Biology Department, Brookhaven National Laboratory, Upton, New York 11973, and Department of Biochemistry and Molecular Biology, College of Medicine, University of South Florida, and H. Lee Moffitt Cancer Center and Research Institute, Tampa, Florida 33612

Received March 29, 2001; Revised Manuscript Received September 19, 2001

ABSTRACT: Cytochrome b_5 reductase (cb5r) (EC 1.6.6.2) catalyzes the reduction of two molecules of cytochrome b_5 using NADH as the physiological electron donor. The structure of pig cb5r at 2.4 Å resolution was previously reported in the literature, but it was inconsistent with the biochemistry; for example, K83 and C245 were both implicated in the mechanism, but were not located at the active site. To address this problem, we have determined the structures of cb5r from rat at 2.0 Å resolution and in a complex with NAD^+ at 2.3 Å resolution. We found significant differences throughout the rat structure compared to that of pig, including the locations of the lysine and cysteine residues mentioned above. To test the structural models, we made single amino acid substitutions of this lysine and showed that all substitutions produced correctly folded proteins and exhibited normal flavin behavior. However, the apparent k_{cat}(NADH) decreased, and the apparent K_m for NADH increased; the K_m's for cytochrome b_5 were unchanged relative to that of the wild type. The largest effect was for the glutamate-substituted protein, which was further characterized using a charge transfer assay and found to be less efficient at NADH utilization than the wild type. These results are consistent with a role for this lysine in stabilizing the NADH-bound form of cb5r. We have concluded that the pig structure was mistraced in several regions and have reinterpreted mutants in these regions that give rise to the hereditary disease methemoglobinemia.

Cytochrome b_5 reductase (cb5r,[1] EC 1.6.2.2), an enzyme involved in both the microsomal electron transport system and erythrocyte function, catalyzes the transfer of reducing equivalents from NADH to two molecules of cytochrome b_5 (cb5). The enzyme contains a single FAD prosthetic group and exists in two forms, a membrane-bound form (*1*) that is comprised of both a hydrophobic membrane-anchoring region ($M_r \sim 3$ kDa, residues 1−25) and a hydrophilic, catalytic, or diaphorase portion ($M_r \sim 30$ kDa, residues 26−300) and a soluble form (*2*) comprising only the soluble reductase.[2] The soluble form of cb5r exists in circulating erythrocytes and catalyzes methemoglobin reduction (*3*), while the membrane-bound form is embedded in the membranes (endoplasmic reticulum, mitochondria, and nuclear and plasma membranes) of somatic cells and, together with the membrane-bound form of cb5, participates in a variety of metabolic transformations, such as the desaturation and elongation of fatty acids (*3*), specific P450-mediated hydroxylation reactions (*4*), and cholesterol biosynthesis (*5*).

The microsomal form of cb5r has been isolated from a variety of sources, including human (*6*), rabbit (*7*), steer (*8*), rat (*9*), and porcine (*10*) liver, as either the mature amphipathic, detergent-solubilized form or the truncated, hydrophilic FAD-containing domain following limited proteolysis (*11*, *12*). In addition, various bacterial expression systems have been developed for the efficient production of the soluble functional forms of human (*12*), steer (*13*), and rat (*14*) liver cb5r.

The crystal structure of porcine cb5r was reported previously at 2.4 Å resolution (*15*). As predicted, it had a fold similar to that of ferredoxin:$NADP^+$ reductase (FNR), the prototypical member of this family of flavin-dependent oxidoreductases (*16*) that also includes phthalate dioxygenase reductase (*17*), and the flavin domain of assimilatory NADH:nitrate reductase (*18*). However, the structure of porcine cb5r exhibited several differences that were suggested to be

† This work was supported by DoE LDRD Project 00-43 (M.C.B.), Grants GM32696 from the NIH (M.J.B.), and Grants 9708450A and 9910034V from the American Heart Association, Florida/Puerto Rico Affiliate (M.J.B.).

* To whom correspondence should be addressed: Biology Department, Brookhaven National Laboratory, Upton, NY 11973. Phone: (631) 344-3798. Fax: (631) 344-3407. E-mail: bewley@bnl.gov.

‡ Brookhaven National Laboratory.

§ University of South Florida.

|| H. Lee Moffitt Cancer Center and Research Institute.

[1] Abbreviations: cb5r, cytochrome b_5 reductase; cb5, cytochrome b_5; FNR, ferredoxin:$NADP^+$ reductase; PDR, phthalate dioxygenase reductase; NR, nitrate reductase; SDS, sodium dodecyl sulfate; PEG, polyethylene glycol; PAGE, polyacrylamide gel electrophoresis; PCR, polymerase chain reaction; IPTG, isopropyl β-D-thioglucopyranoside; FPLC, fast protein liquid chromatography; TB, terrific broth; NTA, nitrilotriacetic acid; MALDI-TOF, matrix-assisted laser desorption ionization time-of-flight; *m*/*z*, mass/charge ratio; μ, ionic strength; HEPES, 4-(2-hydroxyethyl)piperazine-1-ethanesulfonic acid; MOPS, 3-(*N*-morpholino)propanesulfonic acid; MPD, 2-methyl-2,4-pentanediol; CD, circular dichroism.

[2] The protein is numbered according to the membrane-bound form to be consistent with the majority of the biochemical nomenclature. However, the numbering of the crystal structure of pig cb5r refers to the soluble form of the protein. To prevent any confusion, we have annotated the sequence alignment using both numbering systems.

10.1021/bi0106336 CCC: $20.00
Published on Web 10/20/2001

significant and related to differences in reduced pyridine nucleotide specificity. Key residues that had been identified biochemically as being involved in the mechanism, such as K83 (K110 in the rat form) (*19*) and C245 (C283 in the rat form), were not close to the active site. To examine these discrepancies, we decided to determine the structure of rat cb5r to provide a second model for comparison.

We present the structure of cb5r to 2.0 Å resolution and a complex with NAD^+ to 2.3 Å resolution. These structures are consistent with the biochemistry and the structures of other members of the FNR superfamily. To test the structures, we present a kinetic analysis of site-directed substitutions of K110 in the rat enzyme. In light of the new model, we have reanalyzed the positions of the mutants that have been reported to cause methemoglobinemia in humans and present a discussion of those that are affected by the changes in the structure.

MATERIALS AND METHODS

Materials. Materials for bacterial culture, protein purification, and chemical assays were obtained from standard commercial sources as listed in Marohnic and Barber (*20*). Nucleotide sequencing was performed by the Molecular Biology Core Facility at the H. Lee Moffitt Cancer Center and Research Institute.

Site-Directed Mutagenesis and Protein Purification. K110 mutants of rat cb5r were generated as previously described (*20*) from complementary oligonucleotide primers (35mers) that contained the desired codon change and eliminated a *Drd*I restriction site. Wild-type and mutant cb5r were purified to homogeneity, as previously described (*14*).

Crystallography. Crystals were grown by the sitting drop method. Two microliters of a protein solution and 2 μL of a reservoir solution were mixed over a reservoir of 8% PEG6000 and 5% MPD in 100 mM HEPES (pH 7.5). For data collection, crystals were cooled directly in a stream of liquid nitrogen gas from an Oxford Cryosystems cryostream at 99 K using 42.5% PEG6000 and 5% MPD in 100 mM HEPES (pH 7.5) as a cryoprotectant. Data were collected on beamline x12c at the National Synchrotron Light Source (Brookhaven National Laboratory) using the Brandeis four-cell CCD. A complete dataset to 2.0 Å resolution was collected from a single crystal. The data were indexed and scaled using the HKL Program Suite (*21*) (Table 1). The refined orthorhombic unit cell ($a = 68.08$ Å, $b = 70.67$ Å, and $c = 78.99$ Å) exhibited systematic absences that were consistent with space group $P2_12_12_1$. Native crystals were soaked in a solution containing 40 mM NAD^+ for 1 h and data collected to 2.3 Å resolution as described above. The refined orthorhombic unit cell has the following dimensions: $a = 67.61$ Å, $b = 69.46$ Å, and $c = 78.79$ Å.

The structure of native cb5r was determined by molecular replacement in Amore (*22*) using the protein coordinates of maize nitrate reductase (2CND) as a search model. A single solution was found with an *R*-factor of 45.7% (56.7% for the next highest peak). For completeness, translation searches were performed in all possible space groups for the point group, and the results confirmed that the space group was indeed $P2_12_12_1$. All subsequent refinement steps were carried out with the program CNS (*23*). The model was subjected to rigid body refinement followed by a cycle of simulated annealing (SA) at 3000 K and individual isotropic temperature refinement prior to initial $2F_o - F_c$ map calculation. Subsequent model building and refinement was performed until the model could not be improved, as judged by a reduction in R_{free}. SA omit maps were calculated twice: first after rigid body refinement and then using the coordinates from the penultimate refinement step. Coordinates have been deposited in the Protein Data Bank as entry 1I7P. The structure of cb5r in complex with FAD and NAD^+ was determined by molecular replacement using the protein coordinates of cb5r (1I7P) and refined as described above. The coordinates have been deposited in the Protein Data Bank as entry 1IB0.

Table 1: Data Collection and Structure Refinement Statistics

	native	with NAD^+
data collection statistics		
resolution range (Å)	30.0−2.0	30.0−2.3
R_{merge} (%)	8.6 (21.6)	9.1 (31.5)
completeness (%)	99.8 (99.1)	97.3 (90.4)
$I/\sigma I$	11.5 (3.5)	8.5 (2.4)
redundancy	6.2 (5.3)	4.1 (3.5)
refinement statistics		
resolution range (Å)	30.0−2.0	30.0−2.3
R-factor (%)	21.5	21.8
R_{free} (%)	24.4	26.5
no. of reflections in R_{free}	971	1108
no. of reflections where $I/\sigma I > 0$	23306	15598
no. of protein atoms	2182	2182
no. of FAD atoms	53	53
no. of NAD atoms	0	44
no. of water molecules	148	144
rmsd for bond lengths (Å)	0.011	0.010
rmsd for bond angles (deg)	1.8	1.8

Analysis of the structures of rat and pig cb5r using PROCHECK reported that in rat cb5r, 93% of the residues lie within the core region with the remainder in the allowed region, compared to the structure of pig cb5r, which has only 80% of its torsion angles in the core region and 6% in generous or disallowed regions. The *G*-factors for pig and rat cb5r are −0.95 and 0.66, respectively.

Spectroscopy. UV−visible spectra were obtained using a Hewlett-Packard (Agilent Technologies, Palo Alto, CA) 8453 diode-array spectrophotometer. UV CD spectra were obtained using a JASCO (Easton, MD) J710 spectropolarimeter in 10 mM phosphate buffer, containing 0.1 mM EDTA (pH 7.0), as described previously (*20*). All spectra were corrected for the appropriate buffer contributions and are expressed in terms of molar ellipticities (per molar per centimeter).

Enzyme Activities. NADH-dependent ferricyanide reductase activity which requires only a functional FAD group and NADH-dependent cytochrome b_5 reductase activity which requires functional FAD and heme groups were determined at 25 °C under conditions of constant ionic strength and pH, as previously described (*20*), in 116 mM MOPS buffer ($\mu = 0.05$), containing 0.1 mM EDTA (pH 7.0). NADH-dependent ferricyanide activities were routinely determined at 340 nm in the presence of NADH (100 μM) and ferricyanide (200 μM). NADH concentrations were varied from 2 to 120 μM. NADH-dependent cytochrome b_5 reductase activity was monitored at 423 nm in the presence of NADH (100 μM) and soluble, recombinant rat cytochrome b_5 (50 μM). Cytochrome b_5 concentrations were varied from

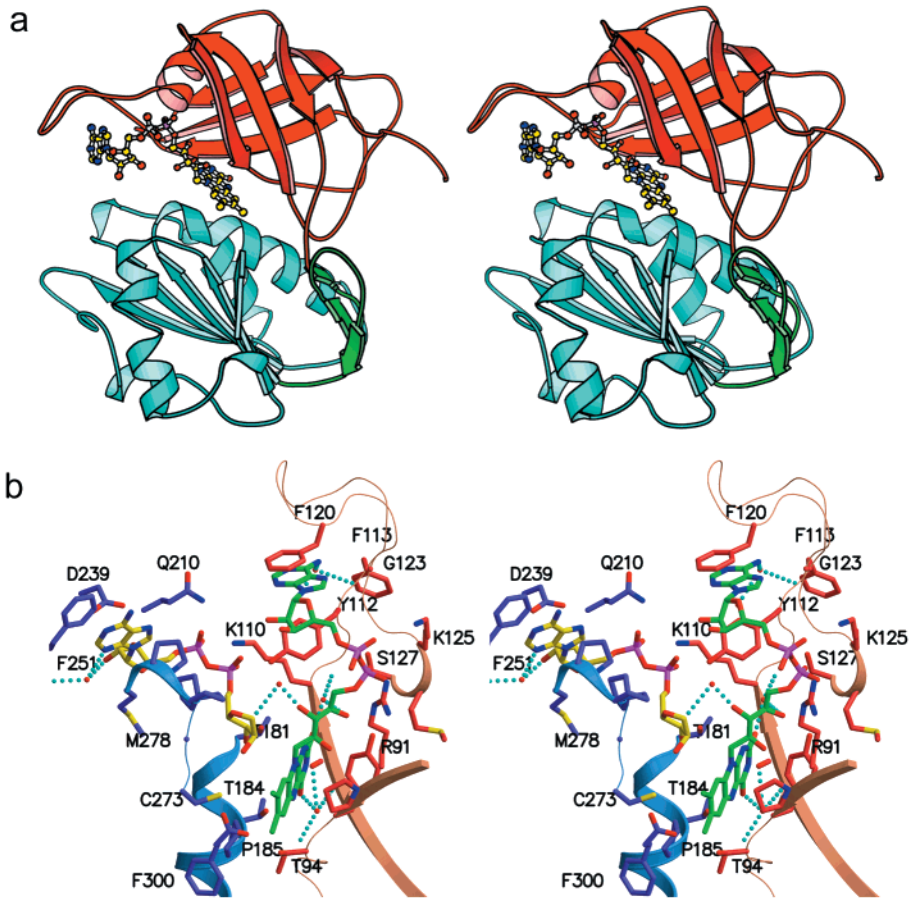

FIGURE 1: Overview of the structure of rat cb5r. (a) Stereo ribbon diagram of rat cb5r showing the elements of each domain. The FAD-binding domain is colored red. Strands in the foreground from top to bottom are 1a, 6, 3, and 4 and those in the background 1b, 2, and 5. The NADH-binding domain is colored blue. Strands from top to bottom are in the order 3, 2, 1, 4, and 5. The three-stranded linker domain is colored green, and the FAD molecule is shown in a ball-and-stick representation using standard atom colors. (b) Interactions of the FAD and visible region of the NAD. Water-mediated hydrogen bonds are shown as cyan dotted lines. This figure was produced using MOLSCRIPT (*40*), BOBSCRIPT (*41*), and RASTER3D (*42*).

2 to 50 μM. Activities are expressed as initial rates for the oxidation of NADH (micromoles of NADH consumed per minute per nanomole of FAD). Initial rate data were analyzed using the software ENZFIT (Elsevier Biosoft, Ferguson, MO) to extrapolate activities to infinite NADH and cytochrome b_5 concentrations to yield apparent V_{max} and K_m values.

RESULTS AND DISCUSSION

Crystallographic Studies. The crystal structure of the FAD-bound form of soluble rat cb5r has been determined and refined to 2.0 Å resolution. The final model contains residues I33−F300 of the mature protein,[2] an FAD molecule, 148 water molecules, and all residues of the amino-terminal His_4-Met tag used for purification. The purification tag is distant from the active site in the structure and has no measurable effect on the spectroscopic and kinetic data of the recombinant protein.

The structure, shown in Figure 1a, is the classical two-domain arrangement, with an amino-terminal FAD-binding domain (residues 33−147) and a carboxyl-terminal NADH-binding domain (residues 171−300). These two domains are linked by a small, 25-amino acid, three-stranded antiparallel β-sheet (residues 148−170) that may serve as a hinge or spacer region to orient the two domains for the efficient transfer of reducing equivalents from NADH to flavin.

The interactions at the FAD-binding site are shown in Figure 1b. The FAD-binding domain, oriented toward the *si*-face of the isoalloxazine ring of the FAD, is a six-stranded, antiparallel β-barrel (Fβ1a, Fβ1b, and Fβ2−Fβ7) with an ~30° twist of each strand. The barrel is capped by the only α-helix in this domain. A long loop (residues 110−125), located between strand 5 and the α-helix, forms a lid that contributes the majority of interactions of the FAD-binding domain with the adenine dinucleotide moiety of the FAD. Many of these interactions are water-mediated. The NADH-binding domain, which is oriented to the *re*-face of the isoalloxazine ring and interacts with this part of the FAD alone, contains a canonical Rossmann fold (three α/β/α layers that pack into a five-stranded parallel β-sheet in the order 3, 2, 1, 4, 5). The isoalloxazine ring bridges the domains, forming interactions with the loop between strands Fβ3 and Fβ4 (residues 92−110) in the FAD-binding domain and the Nβ1−NαA (residues 181−184) of the NADH-binding domain.

Comparison of the structures of rat and pig cb5r suggested differences. To examine these further, we used the protein coordinates of pig cb5r (1NDH) as a search model and followed the same procedure. From these maps, it was immediately obvious that some regions were out of register in pig cb5r compared to the rat structure (Figure 2). Subsequent analysis of the structure of pig cb5r, using

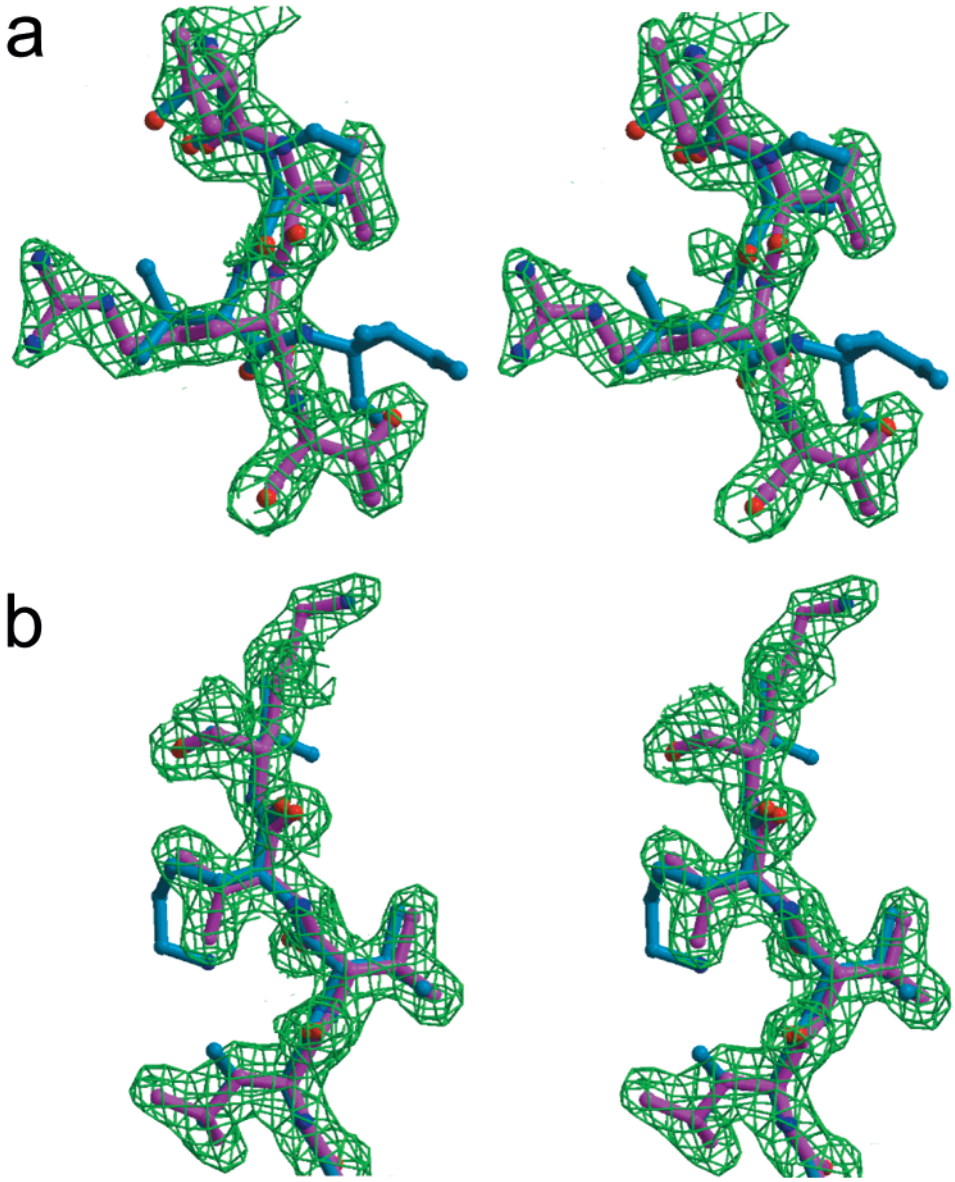

FIGURE 2: Simulated annealing omit maps showing mistraced regions in the structure of pig cb5r. (a) ^{167}VVRT^{170} of rat and ^{137}SPV^{140}I of pig cb5r. The structure of pig is misaligned in this region by two residues with respect to the rat structure. The equivalent sequence from rat (VVRT) is VIKT in pig. (b) The ^{107}LVV^{100}K sequence of rat and the ^{80}VVK^{83}V sequence of pig are shown. This region is involved in FAD cofactor binding and is misaligned by one residue in the pig structure. In each case, the composite omit map electron density is colored green, and rat and pig structures are colored in magenta and cyan, respectively. Nitrogen and oxygen atoms are colored blue and red, respectively. This figure was produced using MOLSCRIPT (*40*), BOBSCRIPT (*41*), and RASTER3D (*42*).

PROCHECK (*24*), suggested that the structure of pig cb5r had some geometric problems, as reflected by the overall *G*-factor of −0.95. This analysis made worse our concern that the differences reported for the structure of pig cb5r in comparison with other family members were a consequence of a mistraced structure rather than biologically significant. Root-mean-square (rms) deviations between equivalent atoms in pig cb5r and rat cb5r showed three out of register regions that affected 14% of the model. They are highlighted in the sequence alignment in Figure 3b. In some cases, the residues with the highest rms deviations are located at the active site; for example, K110 (K83 in pig), which is conserved in FNR family members, has been implicated in binding the reducing substrate, NADH (*25*). In the structure of pig cb5r, K83 is buried behind the isoalloxazine ring of the FAD cofactor with its side chain directed toward the inside of the structure (Figure 3c) and could not bind directly to NADH (*15*). However, its position in the rat model is displaced by ∼11 Å, and it lies in front of the isoalloxazine ring where it is oriented toward the *re*-face of the cofactor. This places the side chain of K110 in a position where it is accessible to interact with an incoming NADH molecule, as suggested by the biochemistry, and in agreement with the structures of other FNR family members. A second example is C273, which is conserved in all members of the FNR family. It was proposed to be close to the NADH-binding site, although it was not thought to be catalytically essential since mutation to alanine showed an only 80% reduction in enzyme activity compared to that of the wild-type enzyme. However, in the structure of pig cb5r, the Sγ atom of the equivalent residue, C245, is buried in the core of the protein, some ∼14 Å from the active site (Figure 3c). In the structure of rat cb5r, the Sγ atom of C273 is located at the active site, only 4 Å from the C8 atom of the isoalloxazine ring of the FAD molecule,

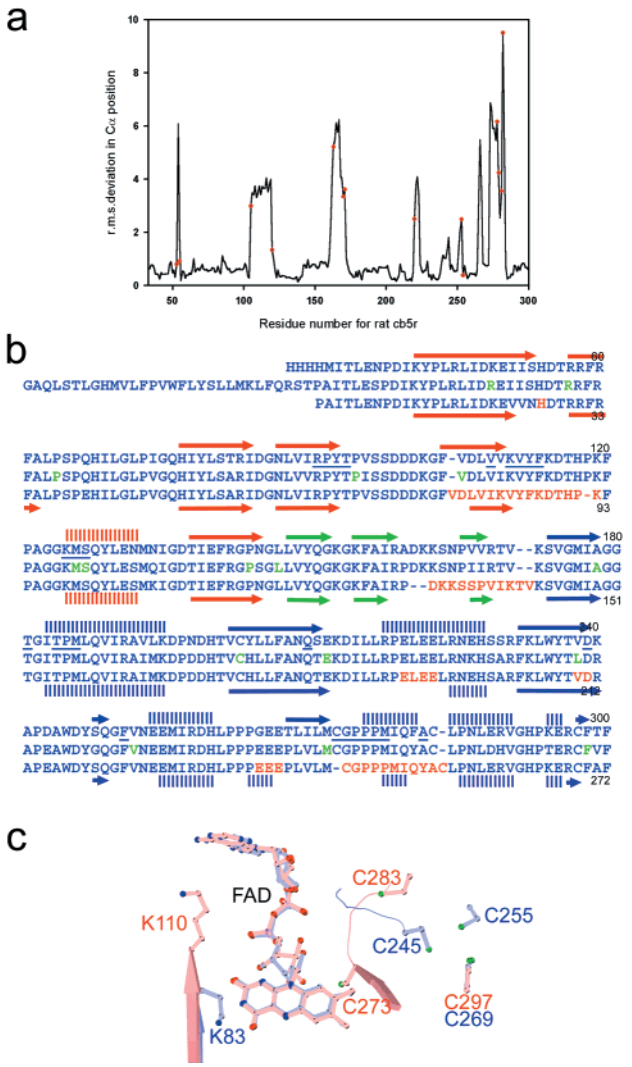

FIGURE 3: Summary of mistraced regions of pig cb5r. (a) The rms coordinate difference of the common Cα atoms between pig cb5r and rat cb5r. Residues in the pig cb5r structure whose backbone torsion angles are outliers in a Ramachandran map are shown as red circles. Specifically, they are N25, D27, V77, F92, K135, T142, V143, E192, N225, E226, M250, I251, Y253, and A254, and are numbered according to the structure of pig cb5r. (b) Sequence alignment of rat, human, and pig cb5r. Rat and human sequences are aligned according to their sequences, whereas the pig amino acid sequence is aligned according to its superposition on the structure of rat cb5r. Residues involved in FAD or NADH binding are underlined on the rat sequence. Residues that are mutated in methemoglobinemia are shown in green on the human cb5r sequence. Regions with rms deviations of >2 Å are highlighted in red on the pig cb5r sequence. The secondary structure elements in rat and pig cb5r are marked above and below their sequences, respectively. They are colored according to the pattern of Figure 1a. Arrows and vertical bars represent β-strands and α-helices, respectively. (c) Relative positions of the active site lysine and cysteine residues. Rat cb5r is colored pink and pig cb5r colored lilac. K110 and C273 in rat are equivalent to K83 and K245 in pig, respectively. Although the FAD molecules are in similar positions, the chain mistraces place these residues in positions where they are unable to interact with the FAD cofactor in a manner that is consistent with the biochemical experiments. This figure was produced using MOLSCRIPT (*40*), BOBSCRIPT (*41*), and RASTER3D (*42*).

and is consistent with the structures of other FNR family members.

These mistraces not only impact the active site but also have consequences in understanding the interaction of cb5r with its physiological partner, cytochrome b_5. For example, the three lysine residues (K41, K125, and K163) have been proposed to interact with the cytochrome b_5 molecule by forming a charge pair interaction (*13*, *26*, *27*). In the structure of rat cb5r, presented here, these residues are located on the same face of the molecule and could simultaneously contact cytochrome b_5. However, in the structure of pig cb5r, K163 is not close to K41 and K125 and is not even on the same face as the other two residues. Thus, it is unlikely that all three lysine residues would be able to make simultaneous interactions with the relatively small cytochrome b_5 protein. This unfortunately brings into question the modeling studies that were published subsequently (*28*).

Structure of Rat cb5r with NAD$^+$ Bound. To understand the chemistry of this structure further, we obtained a structure of rat cb5r in complex with NAD$^+$ to 2.3 Å resolution. The structure contains residues I33−F300, an FAD cofactor, 144 water molecules, and all residues of the N-terminal purification tag. NAD$^+$ binds in an extended conformation along a plateau formed by proline residues 275−277, without any conformational change in the protein or the FAD molecule (Figure 1b). The conformation of the NAD$^+$ is shaped largely by P275 and bends around it. The adenine ring packs parallel to the aromatic ring of F251 in an ~6 Å wide channel created by F251 on one side and the P277 on the other. The diphosphate groups pack against P275; the phosphate oxygen atoms are involved in hydrogen bonds with Q210 Nε2, T181 N, Y112 OH, and K110 Nζ. The nicotinamide proximal ribose packs parallel to the proline ring of P275. The nicotinamide ring is disordered, but there is some diffuse density that suggests it extends out to the solvent. To bind in a productive manner, the sugar and nicotinamide moieties of the NAD and the protein would have to change conformation, since there is insufficient room to accommodate NADH in this conformation. This is consistent with reports that crystals of the NADH-dependent flavoprotein, nitrate reductase, dissolve when they are placed in an NAD$^+$-containing environment (*18*).

To gain insight into the potential productive mode of NADH binding, we studied the published structure of a single-site variant of the prototypical protein in this superfamily, FNR, with NADP$^+$ bound in a productive manner (*29*) (Figure 4a). In the structure of the wild-type enzyme, the carboxyl-terminal tyrosine residue prevents the binding of NADP$^+$ in a productive mode (*16*). When a serine residue is substituted for this tyrosine residue, NADP$^+$ binds productively without causing a conformational change in the protein (*29*). The nicotinamide ring lies at −30° to the *re*-face of the isoalloxazine ring placing the C4 atom ~3 Å from the flavin N5 atom. Visible spectra have shown that the variant and wild-type enzymes have the same geometry with respect to the NADP$^+$, but the wild-type enzyme binds the substrate less tightly. Thus, the tyrosine residue may act as a placeholder for the nicotinamide and has been suggested to flip out of the way to allow the nicotinamide to bind productively. The situation in the NADH-utilizing enzymes, b5r and NR, is slightly different however. When the NAD(P)H-binding domains of rat cb5r and maize NR are superimposed onto that of spinach FNR using the sequence-based fitting algorithm in Swiss PDB Viewer, the carboxyl termini of the NADH-utilizing enzymes are in a different location relative to the isoalloxazine ring (Figure 4a).

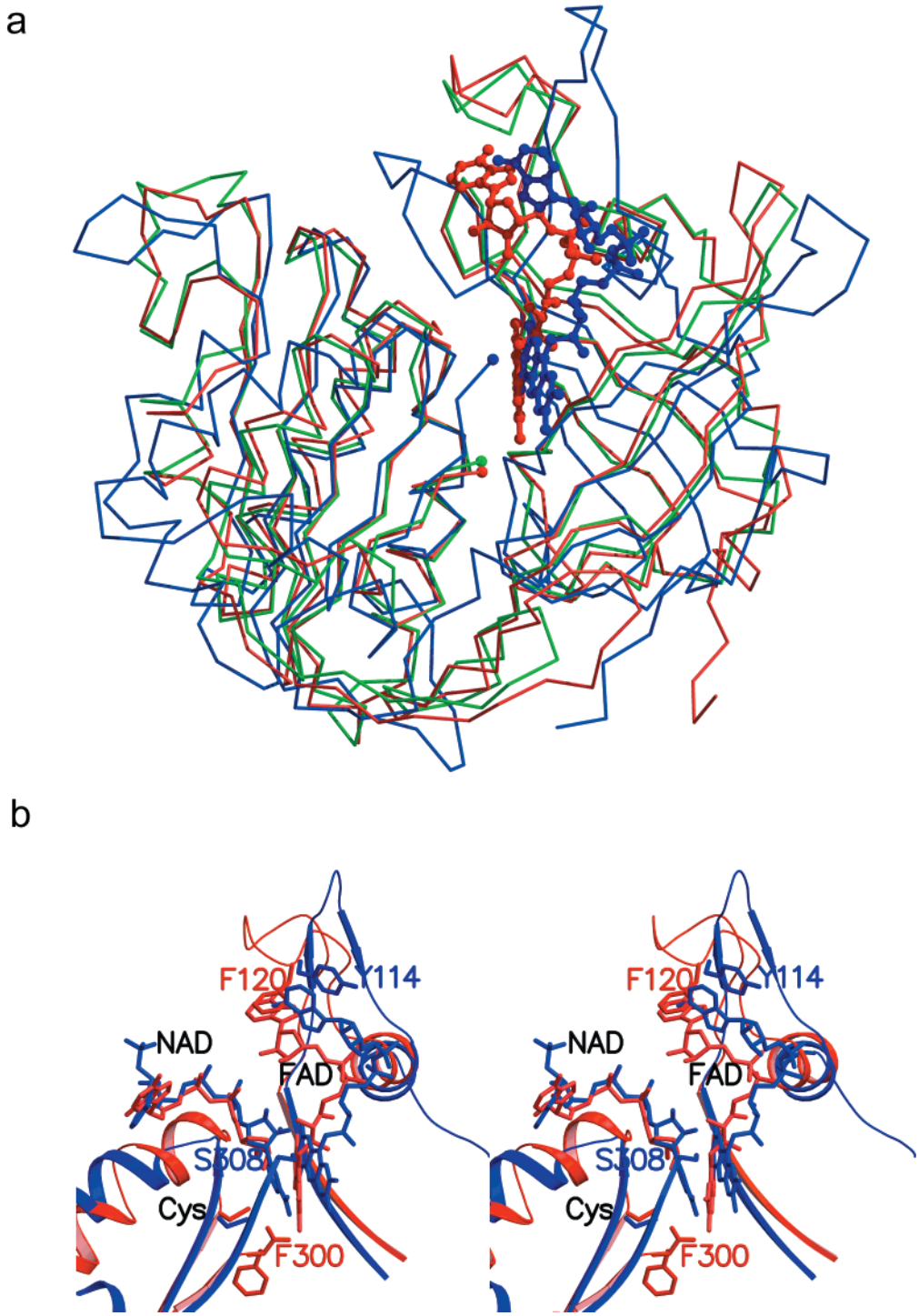

FIGURE 4: Movement of the FAD-binding domain may facilitate binding of NAD^+ in a productive manner in cb5r. (a) Superposition of rat cb5r (red), maize nitrate reductase (blue), and the Y308S mutant of pea FNR (green) using Swiss PDB Viewer. The NAD(P)H-binding domains align well; however, a rotation of the FAD-binding domain of FNR places the FAD cofactor 3−4 Å farther from this domain. The carboxyl terminus in each case is marked with a colored sphere. The FAD molecules for cb5r and FNR are shown in ball-and-stick representations in the appropriate color. (b) A closeup stereoview of the active sites of the Y308S mutant of pea FNR and wild-type cb5r in complex with $NADP^+$ and NAD^+, respectively. They are colored according to the pattern of panel a. On the basis of these structures, we suggest that a small rotation of the FAD-binding domain and a movement of the loop between residues 110 and 125 away from the active site would reposition the FAD cofactor, creating the necessary room for the nicotinamide moiety of the substrate. This figure was produced using MOLSCRIPT (*40*), BOBSCRIPT (*41*), and RASTER3D (*42*).

Whereas in FNR the plane of the aromatic ring is parallel to the *re*-face of the isoalloxazine ring, at a distance of ~3 Å, in b5r the aromatic ring is perpendicular to the plane of the isoalloxazine ring, some ~9 Å from N5 of the FAD (Figure 4b). Further inspection shows that the NAD(P)H-binding domain superimposes well, but there is a twisting motion required to superimpose the FAD-binding domain. In addition, the two loops that form the majority of interactions with the FAD in this domain are in different conformations in the two structures. One consequence of this is that the FAD cofactor is 4−5 Å farther from the NAD(P)H-binding domain in FNR than in cb5r, as shown in Figure 4b. For example,

Table 2: Initial Rate Parameters for the NADH-Dependent Ferricyanide and NADH-Dependent Cytochrome b_5 Activities of Rat cb5r K110 Variants

	NADH-dependent ferricyanide activity			NADH cytochrome b_5 activity		
cb5r	$k_{cat(app)}$ (s^{-1})	$K_{m(app)}$(NADH) (μM)	k_{cat}/K_m (s^{-1} M^{-1})	$k_{cat(app)}$ (s^{-1})	$K_{m(app)}$(cb_5) (μM)	k_{cat}/K_m (s^{-1} M^{-1})
wild type	800 ± 8	6 ± 1	$(1.3 \pm 0.1) \times 10^8$	270 ± 25	10 ± 3	$(2.7 \pm 1.0) \times 10^7$
K110R	470 ± 5	5 ± 0	$(1.0 \pm 0.2) \times 10^8$	200 ± 40	9 ± 3	$(2.3 \pm 1.4) \times 10^7$
K110H	340 ± 8	50 ± 10	$(6.3 \pm 1.9) \times 10^6$	110 ± 15	12 ± 3	$(9.6 \pm 4.7) \times 10^6$
K110A	270 ± 25	380 ± 60	$(7.2 \pm 4.5) \times 10^5$	90 ± 2	9 ± 0	$(10.0 \pm 4.3) \times 10^6$
K110E	120 ± 23	370 ± 120	$(3.2 \pm 2.0) \times 10^5$	1 ± 1	4 ± 1	$(4.0 \pm 2.0) \times 10^5$
K110Q	40 ± 5	760 ± 130	$(5.3 \pm 3.9) \times 10^4$	4 ± 1	3 ± 1	$(1.3 \pm 0.40) \times 10^6$

the isoalloxazine ring is ~4 Å from the Sγ atom of C273 in rat cb5r, whereas in FNR the isoalloxazine ring is ~9 Å from the Sγ atom of the equivalent cysteine, C266. Thus, a conformational change in these loops would change the shape of the active site, providing the necessary room for the nicotinamide ring to position itself for hydride transfer. In rat cb5r, one of the loops is involved in a crystal contact with a symmetry-related molecule, and so our observation that crystals crack when exposed to NAD for extended periods of time and do not bind in a productive manner when exposed for a shorter period of time is consistent with this hypothesis. To test this idea further, we are currently attempting to cocrystallize cb5r with NAD^+.

Site-Directed Mutagenesis of K110. On the basis of the acetylation studies of lysine residues and kinetic characterization of K110 mutants that either maintained or abolished positive charge, Strittmatter and co-workers suggested a role for K110 in NADH binding (*8*, *19*, *25*). However, in the crystal structure of pig cb5r, this residue was not located at the active site. To further test the two structures of cb5r, we constructed a set of single-site variants of K110 in rat cb5r, in which the lysine residue was replaced with arginine, histidine, glutamic acid, glutamine, and alanine, respectively, and tested their catalytic properties. In all cases, the purified variants were of appropriate mass and contained FAD as the sole prosthetic group as shown by MALDI-TOF mass spectroscopy and UV−visible spectroscopy (results not shown). UV CD spectra and thermal denaturation curves (results not shown) were similar to those of the wild-type enzyme, indicating that these substitutions did not significantly alter the folding or stability of either the enzyme or the FAD prosthetic group. In addition to binding its physiological partner, NADH, and cytochrome b_5, cb5r also exhibits an intrinsic NADH-dependent ferricyanide reductase activity that requires the presence of a functional FAD prosthetic group alone. Thus, these two activities, which are measured separately, can be used to uncouple the NADH and cytochrome b_5 binding properties of the enzyme. Initial rate kinetic analyses of both activities for the wild-type and K110 mutant enzymes are shown in Table 2. In agreement with the previous observations of Strittmatter for bovine cb5r (*19*), all mutations adversely affect enzyme turnover, while the loss of positive charge significantly reduces the affinity of the enzyme for NADH. This result is consistent with the location of K110 at the active site in the crystal structure of rat cb5r and its interaction with one of the phosphate oxygen atoms of bound NAD^+. None of these mutants had any significant affect on the K_m for cytochrome b_5, suggesting that K110 may not make a major contribution to cytochrome b_5 binding.

The largest effect was in the K110Q variant, which was investigated further. We compared the abilities of the wild-type and K110Q forms of rat cb5r to form the characteristic charge transfer complex between reduced flavin ($FADH_2$) and NAD^+ that has been observed during reductive titrations of FNR family members such as cb5r (*10*, *30*), FNR (*31*), and the FAD domain of corn NR (*32*). The formation of these charge transfer species in various flavoproteins has been suggested to be characteristic of flavin nucleotide stacking (*29*, *33*). The characteristic spectral shift for wild-type cb5r is shown in Figure 5a. The K110Q mutant exhibited significantly different absorbance changes that were most apparent in the long wavelength region of the spectrum (Figure 5b). Although the charge transfer complex was still formed, the total absorbance at 800 nm was approximately half of that of the wild-type enzyme, suggesting either that the K110Q variant forms a less effective interaction between the reduced flavin and NAD^+ in the fully formed complex or that the spectra are sampling the fraction of bound NAD in which the nicotinamide and flavin are in contact (*29*). These mutagenesis results, in conjunction with the crystal structures presented above, suggest that K110 plays an important role in correctly orienting the binding of the reduced pyrimidine nucleotide substrate to promote efficient reduction of the flavin prosthetic group.

Hereditary Methemoglobinemia. Methemoglobinemia is a metabolic disease that results directly from a deficiency of NADH−cytochrome b_5 reductase. There are two types of cb5r deficiency (*34*). In the type I disease, in which soluble cb5r activity is reduced, the only symptom is well-tolerated cyanosis, which generally gives rise to mild complaints such as headaches, fatigue, and shortness of breath during exercise. In the type II disease, the enzyme defect involves both soluble and microsomal cytochrome b_5 reductase in both red cells and leukocytes and causes mental deficiency, which may be related to the major role played by the cytochrome b_5 system in the desaturation of fatty acids. To date, there are a total of 25 different mutations in cb5r that give rise to methemoglobinemia, the majority of which have been previously analyzed in a structural context (*35*). Therefore, we will limit our discussion to three mutants: M126V which has been reported very recently (*36*) and V105M and V253M which have a different interpretation in light of the new structure.

M126 forms part of the FAD-binding site. The backbone amide nitrogen atom of M126 and the guanidine group of R91 form hydrogen bonds to the phosphate oxygen atoms of the FAD cofactor. The side chain atoms of M126 are housed in a hydrophobic pocket that is formed by the side

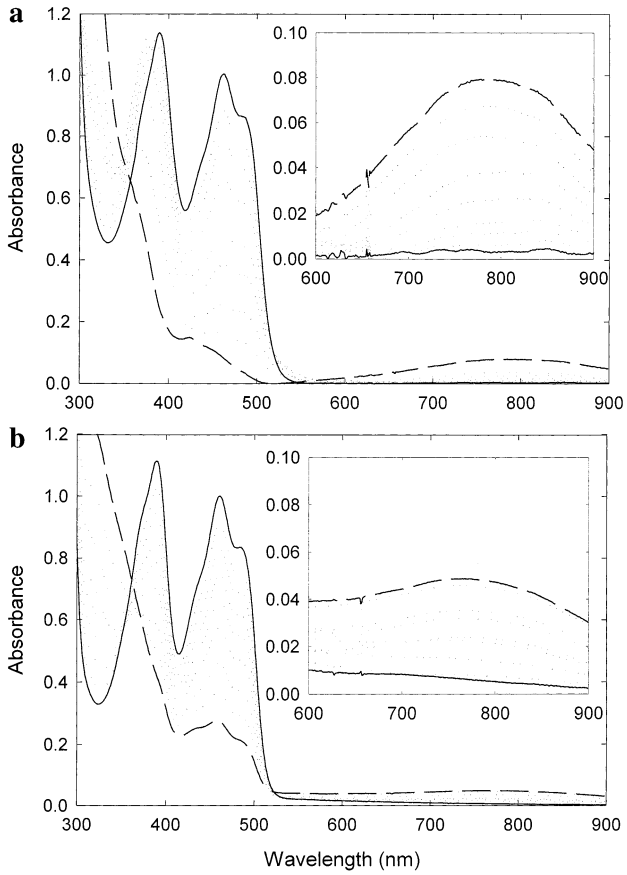

FIGURE 5: Reductive titrations of wild-type cb5r and the K110Q mutant. (a) UV−visible spectra were obtained during the course of an anaerobic reductive titration of the wild-type cb5r (9.4 μM FAD) in the presence of NAD^+ (2 mM) in 116 mM MOPS buffer, containing 0.1 mM EDTA (pH 7.0) using sodium dithionite as a reductant. Individual spectra were recorded following the addition of small aliquots of a dithionite solution following the cessation of all absorbance changes. The inset shows the absorbance changes occurring in the near-IR region of the spectra. (b) UV−visible spectra obtained during the course of a reductive titration of the K110Q variant (94 μM FAD) as described for the wild-type enzyme.

chain atoms of L80, T82, V89, Y93, Y129, I139, and the hydrophobic atoms of R91. Thus, M126V is likely to significantly perturb the binding of the FAD, to produce a nonfunctional enzyme that gives rise to the type II disease.

V105M is located in a local hotspot and involves the cluster of mutations L72P (*37*), P95H (*38*), and V105M (*39*) that are localized in the hydrophobic core of the FAD-binding domain, ~6−9 Å from the active site. L70 and I78 also contribute to the hydrophobic environment. The locations of these residues suggest that this is a region of local plasticity. V105 was in an incorrectly traced region of the pig cb5r structure, and so this cluster was previously not obvious.

The significance of V252M only becomes clear in the structure of cb5r in complex with NAD^+. In the native structure, it is located in a surface-exposed loop. However, in the structure of the complex, we discover that the loop forms part of the NAD^+-binding site, helping to position the side chain of F251 over the adenine of the substrate. In addition, the amide nitrogen atom of V252 forms a water-mediated hydrogen bond to the AO2* atom of NAD^+. The valine is located in a closely packed hydrophobic environment formed by I177, L206, A208, T237, M256, M278, and C283. The addition of a much bulkier methionine residue would likely disrupt the local conformation of the loop, resulting in a less tightly bound substrate.

The structure of rat NADH-dependent cytochrome b_5 reductase presented here is consistent with the biochemical experiments reported previously in the literature. It provides a new model for cb5r that is consistent with the other members of the FNR superfamily. The structure of the complex with NAD^+ shows the mode of binding of the adenine diphosphate ribose portion. Superposition with FNR suggests a possible substrate-induced conformational change for productive binding of the nicotinamide moiety. In the absence of a structure for human cb5r, this work provides a new template for homology modeling and interpretation of the mutations that lead to the disease methemoglobinemia.

REFERENCES

1. Spatz, L., and Strittmatter, P. (1973) *J. Biol. Chem. 248*, 793−799.
2. Passon, P. G., and Hultquist, D. E. (1972) *Biochim. Biophys. Acta 275*, 62−66.
3. Hultquist, D. E., and Passon, P. G. (1971) *Nat. New Biol. 229*, 252−254.
4. Hildebrandt, A., and Estabrook, R. W. (1971) *Arch. Biochem. Biophys. 143*, 66−79.
5. *5.* Reddy, V., Kupfer, D., and Capsi, E. (1977) *J. Biol. Chem. 252*, 2797−2801.
6. Yubisui, T., Miyata, T., Iwanaga, S., Tamura, M., and Takeshita, M. (1986) *J. Biochem. 99*, 407−422.
7. Mihara, K., and Sato, R. (1975) *J. Biochem. 78*, 1057−1073.
8. Loverde, A., and Strittmatter, P. (1968) *J. Biol. Chem. 243*, 5779−5787.
9. Takesue, S., and Omura, T. (1970) *J. Biochem. 67*, 267−276.
10. Iyanagi, T. (1977) *Biochemistry 16*, 2725−2730.
11. Schafer, D. A., and Hultquist, D. E. (1980) *Biochem. Biophys. Res. Commun. 95*, 381−387.
12. Tomatsu, S., Kobayashi, Y., Fukumaki, Y., Yubisui, T., Orii, T., and Sakaki, Y. (1989) *Gene 80*, 353−361.
13. Strittmatter, P., Kittler, J. M., Coghill, J. E., and Ozols, J. (1992) *J. Biol. Chem. 267*, 2519−2523.
14. Barber, M. J., and Quinn, G. B. (1996) *Protein Expression Purif. 8*, 41−47.
15. Nishida, H., Inaka, K., Yamanaka, M., Kaida, S., Kobayashi, K., and Miki, K. (1995) *Biochemistry 34*, 2763−2767.
16. Karplus, P. A., Daniels, M. J., and Herriott, J. R. (1991) *Science 251*, 60−66.
17. Correll, C. C., Batie, C. J., Ballou, D. P., and Ludwig, M. L. (1992) *Science 258*, 1604−1610.
18. Lu, G., Lindqvist, Y., Schneider, G., Dwivedi, U., and Campbell, W. H. (1995) *J. Mol. Biol. 248*, 931−948.
19. Strittmatter, P., Kittler, J. M., and Coghill, J. E. (1992) *J. Biol. Chem. 267*, 20164−20167.
20. Marohnic, C., and Barber, M. J. (2001) *Arch. Biochem. Biophys. 389*, 223−233.
21. Otwinowski, Z., and Minor, W. (1997) in *Methods in Enzymology* (Carter, C. W., and Sweet, R. M., Eds.) pp 307−326, Academic Press, San Diego.
22. Collaborative Computational Project Number 4 (1991) *The SRC(UK) Collaborative Computing Project No. 4: A Suite of Programs for Protein Crystallography*, Daresbury Laboratory, Warrington, U.K.
23. Brunger, A. T., Adams, P. D., Clore, G. M., DeLano, W. L., Gros, P., Grosse-Kunstleve, R. W., Jiang, J. S., Kuszewski, J., Nilges, M., Pannu, N. S., Read, R. J., Rice, L. M., Simonson, T., and Warren, G. L. (1998) *Acta Crystallogr. D54*, 905−921.
24. Laskowski, R. A., MacArthur, M. W., Moss, D. M., and Thornton, J. M. (1993) *J. Appl. Crystallogr. 26*, 283−291.

25. Hackett, C. S., Novoa, W. B., Kensil, C. R., and Strittmatter, P. (1988) *J. Biol. Chem. 263*, 7539−7543.
26. Strittmatter, P., Hackett, C. S., Korza, G., and Ozols, J. (1990) *J. Biol. Chem. 265*, 21709−21713.
27. Shirabe, K., Nagai, T., Yubisui, T., and Takeshita, M. (1998) *Biochim. Biophys. Acta 1384*, 16−22.
28. Nishida, H., and Miki, K. (1996) *Proteins 26*, 32−41.
29. Deng, Z., Aliverti, A., Zanetti, G., Arakaki, A. K., Ottado, J., Orellano, E. G., Clacaterra, N. B., Ceccarelli, E. D., Carrillo, N., and Karplus, P. A. (1999) *Nat. Struct. Biol. 6*, 847−852.
30. Iyanagi, T., Watanabe, S., and Anan, K. F. (1984) *Biochemistry 23*, 1418−1425.
31. Aliverti, A., Gadda, G., Ronchi, S., and Zanetti, G. (1991) *Eur. J. Biochem. 198*, 21−24.
32. Ratnam, K., Shiraishi, N., Campbell, W. H., and Hille, R. (1995) *J. Biol. Chem. 270*, 24067−24072.
33. Massey, V., and Ghisla, S. (1974) *Ann. N.Y. Acad. Sci. 227*, 446−465.
34. Vives-Corrons, J. L., Pujades, A., Vela, E., Corretger, J. M., Leroux, A., and Kaplan, J. C. (1978) *Acta Haematol. 59*, 348−353.
35. Dekker, J., Eppink, M. H. M., van Dwieten, R., de Rijk, T., Remacha, A. F., Law, L. K., Li, A. M., Cheung, K. L., Berkel, J. H., and Roos, D. (2001) *Blood 97*, 1106−1114.
36. Kugler, W., Pekrun, A., Lapse, P., Erdlenbruch, B., and Lakomek, M. (2001) *Hum. Mutat. 402*, 1−5.
37. Wu, Y. S., Huang, C. H., Wan, Y., Huang, Q. J., and Zhu, Z. Y. (1998) *Br. J. Haematol. 102*, 575−577.
38. Manabe, J., Arya, R., Sumimoto, H., Yubisui, T., Bellingham, A. J., Layton, D. M., and Fukumaki, Y. (1996) *Blood 88*, 3208−3215.
39. Shirabe, K., Yubisui, T., Borgese, N., Tang, C. Y., Hultquist, D. E., and Takeshita, M. (1992) *J. Biol. Chem. 267*, 20416−20421.
40. Kraulis, P. J. (1991) *J. Appl. Crystallogr. 24*, 946.
41. Esnouf, R. M. (1997) *J. Mol. Graphics 15*, 132−134.
42. Merritt, E. A., and Bacon, D. J. (1997) in *Methods in Enzymology* (Carter, C. W., and Sweet, R. M., Eds.) pp 505−524, Academic Press, San Diego.

BI0106336